Transp Porous Med (2007) 68:389–411
DOI 10.1007/s11242-006-9050-y

ORIGINAL PAPER

A sequential numerical chemical compositional simulator

Zhangxin Chen · Yuanle Ma · Guo Chen

Received: 13 September 2004 / Accepted: 18 August 2006 / Published online: 3 November 2006

Abstract Chemical flooding in the petroleum industry has a larger scale of oil recovery efficiency than water flooding. On the other hand, it is far more technical, costly, and risky. Numerical reservoir simulation can be employed to conduct mechanism study, feasibility evaluation, pilot plan optimization, and performance prediction for chemical flooding to improve recovery efficiency and reduce operational costs. In this article, we study numerical simulation of chemical flooding such as alkaline, surfactant, polymer, and foam (ASP+foam) flooding. The main displacement mechanisms in this type of flooding are interfacial tension lowering, capillary desaturation, chemical synergetic effects, and mobility control. The model of chemical flooding involves such physicochemical phenomena as dispersion, diffusion, adsorption, chemical reactions, and in situ generation of surfactant from acidic crude oil. The numerical simulator is based on a sequential solution approach that solves both pressure and compositions implicitly, and is applied to three experiments, a chemical flow without mass transfer between phases, a laboratory sandstone core, and an ASP+foam displacement problem with mass transfer, and to a real oilfield. A comparison with UTCHEM is also performed. These applications and comparison indicate that this numerical simulator is practical, efficient, and accurate for simulating complex chemical flooding processes.

Keywords Petroleum reservoir · Chemical flooding · Enhanced oil recovery · Chemical compositional flow · Contaminant flow · Enhanced remediation · Numerical experiment

Z. Chen (✉) · Y. Ma · G. Chen
Center for Scientific Computation, Box 750156, Southern Methodist University, Dallas, TX 75275-0156, USA
e-mail: zchen@mail.smu.edu.

Y. Ma · G. Chen
INET, Tsinghua University, Beijing 100084, P. R. China
e-mail: mayl@tsinghua.edu.cn.

Mathematics subject classifications (2000) 35K60 · 35K65 · 76S05 · 76T05

1 Introduction

Enhanced oil recovery (EOR) is oil recovery by injecting materials that are not normally present in a petroleum reservoir. One of the important methods in EOR is chemical flooding such as alkaline, surfactant, polymer, and foam (ASP+foam) flooding. The injection of these chemical species reduces fluid mobility to improve the sweep efficiency of the reservoir, i.e., increases the volume of the permeable medium contacted at any given time (Lake 1989). While chemical flooding in the petroleum industry has a larger scale of oil recovery efficiency than water flooding, it is far more technical, costly, and risky. The displacement mechanisms in this type of flooding involve interfacial tension lowering, capillary desaturation, chemical synergetic effects, and mobility control, and its flow and transport model describes such physicochemical phenomena as dispersion, diffusion, adsorption, chemical reactions, and in-situ generation of surfactant from acidic crude oil.

In this article, we develop and study a multicomponent, multiphase model for ASP+foam flooding. This model describes synergetic effects in the form of an interfacial tension function, the foam flow resistance in the function of surfactant and oil concentrations, capillary pressure, permeability, gas–liquid ratio, and gas velocity, and the phase behavior in terms of equations of state. The balance equations are the mass balance equation for each chemical species, the aqueous phase pressure equation, and the energy balance equation. The major physical variables modeled are density, viscosity, velocity-dependent dispersion, molecular diffusion, adsorption, interfacial tension, relative permeability, capillary pressure, capillary trapping, cation exchange, and polymer and gel properties such as permeability reduction, inaccessible pore volume, and non-Newtonian rheology (Pope and Nelson 1978). The phase mobilization is described through entrapped phase saturation and relative permeability dependence on the trapping number. Chemical reactions include aqueous electrolyte chemistry, precipitation/dissolution of minerals, ion-exchange reactions with the matrix (the geochemical option), reactions of acidic components of oil with the bases in the aqueous solution, and polymer reactions with cross-linking agents to form gel (Bhuyan et al. 1991).

A discretization scheme based on the block-centered finite difference method (equivalently, a mixed finite element method on rectangular grids(Russell and Wheeler 1983) is utilized to the numerical solution of the mathematical model. By a careful choice of the primary unknowns, a sequential solution approach is used to solve the system of coupled equations for this model. The sequential approach splits the coupled system of nonlinear governing equations of this model up into individual equations and solves each of these equations separately and implicitly. This approach is extended from the IMPEC (i.e., implicit in pressure and explicit in composition) solution approach used in UTCHEM (Delshad et al. 2000) for compositional simulation of chemical flooding. The numerical simulation can be employed to conduct mechanism study, feasibility evaluation, pilot plan optimization, and performance prediction for chemical flooding to improve oil recovery efficiency and reduce operational costs. Our numerical simulator is applied to three experiments, a chemical flow without mass transfer between phases, a laboratory sandstone core, and an ASP+foam displacement problem with mass transfer, and to a real oilfield. A comparison with UTCHEM is also performed. These experiments indicate that this numerical

simulator is practical, reliable, and accurate for simulating complex chemical flooding processes, and that the sequential approach is much more efficient and accurate than the IMPEC.

The rest of this article is organized as follows. In the next section, we review the differential equations governing chemical flooding. The numerical solution scheme is briefly presented in Sect. 3. Numerical experiments are given in Sect. 4, and an oilfield application is presented in Sect. 5. Finally, we conclude with a few remarks in the last section.

We mention that the mathematical model and numerical simulator developed in this article can be also used to study contaminant transport and surfactant enhanced aquifer remediation of pollutants. The governing differential equations, chemical reactions, and phase behavior in EOR are similar to those in contaminant transport and remediation. While the methods and techniques studied focus on the former, the technology transfer can be easily carried out for the latter.

2 Basic differential equations

The governing differential equations for a compositional model of chemical flooding consist of a mass conservation equation for each component, an energy equation, Darcy's law, an overall mass conservation or continuity equation for pressure, and phase behavior. These equations will be developed under the assumptions: local thermodynamic equilibrium, immobile solid phase, Fickian dispersion, ideal mixing, slightly compressible soil and fluids, and Darcy's law.

We consider the general case where N_c chemical components form N_p phases. Let ϕ and $\mathbf{k}$ denote the porosity and permeability of a porous medium $\Omega \subset \Re^3$, and ρ_α, S_α, μ_α, p_α, $\mathbf{u}_\alpha$, and $k_{r\alpha}$ be the density, saturation, viscosity, pressure, volumetric velocity, and relative permeability of the α phase, $\alpha = 1, 2, \ldots, N_p$, respectively. The mass conservation for component i is expressed in terms of the overall concentration of this component per unit pore volume:

$$\frac{\partial}{\partial t}(\phi \tilde{c}_i \rho_i) = -\nabla \cdot \left(\sum_{\alpha=1}^{N_p} \rho_i \left[c_{i\alpha} \mathbf{u}_\alpha - \mathbf{D}_{i\alpha} \nabla c_{i\alpha} \right] \right) + q_i, \quad i = 1, 2, \ldots, N_c, \tag{1}$$

where the overall concentration $\tilde{c}_i$ is the sum over all phases, including the adsorbed phases:

$$\tilde{c}_i = \left(1 - \sum_{j=1}^{N_{cv}} \hat{c}_j \right) \sum_{\alpha=1}^{N_p} S_\alpha c_{i\alpha} + \hat{c}_i, \quad i = 1, 2, \ldots, N_c, \tag{2}$$

N_{cv} is the total number of volume-occupying components (such as water, oil, surfactant, and air), $\hat{c}_i$, ρ_i, and q_i are the adsorbed concentration, mass density, and source/sink term of component i, and $c_{i\alpha}$ and $\mathbf{D}_{i\alpha}$ are the concentration and diffusion–dispersion tensor of component i in phase α, respectively.

The density ρ_i is related to a reference phase pressure p_r by

$$C_i = \frac{1}{\rho_i} \frac{\partial \rho_i}{\partial p_r}\Big|_T,$$

at a fixed temperature T, where $\mathcal{C}_i$ is the compressibility of component i. For a slightly compressible fluid, ρ_i is given by

$$\rho_i = \rho_i^o\big(1 + \mathcal{C}_i^o(p_r - p_r^o)\big), \tag{3}$$

where $\mathcal{C}_i^o$ and ρ_i^o are the constant compressibility and the density at the reference pressure p_r^o, respectively.

The diffusion–dispersion tensor $\mathbf{D}_{i\alpha}$ for multiphase flow is defined by

$$\mathbf{D}_{i\alpha}(\mathbf{u}_\alpha) = \phi\left\{S_\alpha d_{i\alpha}\mathbf{I} + |\mathbf{u}_\alpha|\left(d_{l\alpha}\mathbf{E}(\mathbf{u}_\alpha) + d_{t\alpha}\mathbf{E}^\perp(\mathbf{u}_\alpha)\right)\right\}, \tag{4}$$

where $d_{i\alpha}$ is the molecular diffusion coefficient of component i in phase α, $d_{l\alpha}$ and $d_{t\alpha}$ are, respectively, the longitudinal and transverse dispersion coefficients of phase α, $|\mathbf{u}_\alpha|$ is the Euclidean norm of $\mathbf{u}_\alpha$: $|\mathbf{u}_\alpha| = \sqrt{u_{1\alpha}^2 + u_{2\alpha}^2 + u_{3\alpha}^2}$, $\mathbf{u}_\alpha = (u_{1\alpha}, u_{2\alpha}, u_{3\alpha})$, $\mathbf{E}(\mathbf{u}_\alpha)$ is the orthogonal projection along the velocity:

$$\mathbf{E}(\mathbf{u}_\alpha) = \frac{1}{|\mathbf{u}_\alpha|^2}\begin{pmatrix} u_{1\alpha}^2 & u_{1\alpha}u_{2\alpha} & u_{1\alpha}u_{3\alpha} \\ u_{2\alpha}u_{1\alpha} & u_{2\alpha}^2 & u_{2\alpha}u_{3\alpha} \\ u_{3\alpha}u_{1\alpha} & u_{3\alpha}u_{2\alpha} & u_{3\alpha}^2 \end{pmatrix},$$

$\mathbf{E}^\perp(\mathbf{u}_\alpha) = \mathbf{I} - \mathbf{E}(\mathbf{u}_\alpha)$, and $\mathbf{I}$ is the identity matrix, $i = 1, 2, \ldots, N_c$, $\alpha = 1, 2, \ldots, N_p$. The source/sink term q_i combines all rates for component i and is expressed by

$$q_i = \phi\sum_{\alpha=1}^{N_p} S_\alpha r_{i\alpha} + (1-\phi)r_{is} + \tilde{q}_i, \tag{5}$$

where $r_{i\alpha}$ and r_{is} are the reaction rates of component i in the α fluid phase and rock phase, respectively, and $\tilde{q}_i$ is the injection/production rate of the same component per bulk volume. The volumetric velocity $\mathbf{u}_\alpha$ is given by Darcy's law

$$\mathbf{u}_\alpha = -\frac{1}{\mu_\alpha}\mathbf{k}k_{r\alpha}(\nabla p_\alpha - \rho_\alpha \wp \nabla z), \qquad \alpha = 1, 2, \ldots, N_p, \tag{6}$$

where $\wp$ is the magnitude of the gravitational acceleration and z is the depth.

The energy conservation equation reads

$$\frac{\partial}{\partial t}\left(\phi\sum_{\alpha=1}^{N_p}\rho_\alpha S_\alpha U_\alpha + (1-\phi)\rho_s C_s T\right) + \nabla\cdot\sum_{\alpha=1}^{N_p}\rho_\alpha \mathbf{u}_\alpha H_\alpha - \nabla\cdot(k_T\nabla T) = q_c - q_L, \tag{7}$$

where T is temperature, U_α and H_α are the specific internal energy and the enthalpy of the α-phase (per unit mass), ρ_s and C_s are the density and the specific heat capacity of the solid, k_T represents the total thermal conductivity, q_c denotes the heat source item, and q_L indicates the heat loss to overburden and underburden. In (7), the specific internal energy U_α and the enthalpy H_α of phase α can be computed as follows:

$$U_\alpha = C_{V\alpha}T, \quad H_\alpha = C_{p\alpha}T,$$

where $C_{V\alpha}$ and $C_{p\alpha}$ represent the heat capacities of phase α at constant volume and pressure, respectively.

In the IMPEC or sequential simulation of chemical flooding, a pressure equation for the aqueous phase (e.g., phase 1) is obtained by an overall mass balance on

volume-occupying components. Other phase pressures are evaluated using the capillary pressure functions:

$$p_{c\alpha 1} = p_\alpha - p_1, \qquad \alpha = 1, 2, \ldots, N_p, \tag{8}$$

where $p_{c11} = 0$ for convenience. Introduce the phase mobility

$$\lambda_\alpha = \frac{k_{r\alpha}}{\mu_\alpha} \sum_{i=1}^{N_{cv}} \rho_i c_{i\alpha}, \quad \alpha = 1, 2, \ldots, N_p,$$

and the total mobility

$$\lambda = \sum_{\alpha=1}^{N_p} \lambda_\alpha.$$

Note that

$$\sum_{i=1}^{N_{cv}} \rho_i \mathbf{D}_{i\alpha} \nabla c_{i\alpha} = \mathbf{0}, \quad \sum_{i=1}^{N_{cv}} r_{i\alpha} = \sum_{i=1}^{N_{cv}} r_{is} = 0, \quad \alpha = 1, 2, \ldots, N_p.$$

Now, by adding equations (1) over $i, i = 1, 2, \ldots, N_{cv}$, we obtain the pressure equation

$$\phi \mathcal{C}_t \frac{\partial p_1}{\partial t} - \nabla (\lambda \mathbf{k} \nabla p_1) = \nabla \cdot \sum_{\alpha=1}^{N_p} \lambda_\alpha \mathbf{k} (\nabla p_{c\alpha 1} - \rho_\alpha g \nabla z) + \sum_{i=1}^{N_{cv}} \tilde{q}_i, \tag{9}$$

where the total compressibility $\mathcal{C}_t$ is defined by

$$\mathcal{C}_t = \frac{1}{\phi} \frac{\partial}{\partial p_1} \sum_{i=1}^{N_{cv}} \phi \tilde{c}_i \rho_i.$$

Assume that the rock compressibility $\mathcal{C}_R$ at the reference pressure p_r^0 is given by

$$\phi = \phi^o \big(1 + \mathcal{C}_R (p_r - p_r^o)\big), \tag{10}$$

where ϕ^o is the porosity at p_r^o. With $p_r = p_1$ and using (3) and (10), we have

$$\phi \tilde{c}_i \rho_i = \phi^o \tilde{c}_i \rho_i^o \left(1 + (\mathcal{C}_R + \mathcal{C}_i^0)(p_1 - p_1^o) + \mathcal{C}_R \mathcal{C}_i^0 (p_1 - p_1^o)^2\right).$$

Neglecting the higher order term in this equation (due to the slight compressibility of rock and fluid phases), it becomes

$$\phi \tilde{c}_i \rho_i \approx \phi^o \tilde{c}_i \rho_i^o \left(1 + (\mathcal{C}_R + \mathcal{C}_i^0)(p_1 - p_1^o)\right). \tag{11}$$

Applying (11), the total compressibility $\mathcal{C}_t$ is simplified to

$$\mathcal{C}_t = \frac{\phi^o}{\phi} \sum_{i=1}^{N_{cv}} \tilde{c}_i \rho_i^o \left(\mathcal{C}_R + \mathcal{C}_i^0\right). \tag{12}$$

There are more dependent variables than there are differential and algebraic relations; there are formally $N_c + N_{cv} + N_c N_p + 3N_p + 1$ dependent variables: c_i, $\hat{c}_j$, $c_{i\alpha}$, T, $\mathbf{u}_\alpha$, p_α, and S_α, $\alpha = 1, 2, \ldots, N_p$, $i = 1, 2, \ldots, N_c$, $j = 1, 2, \ldots, N_{cv}$. Equations 1 and

6–9 provide $N_c + 2N_p$ independent relations, differential or algebraic; the additional $N_{cv} + N_c N_p + N_p + 1$ relations are given by the following constraints:

$$\begin{aligned}
&\sum_{\alpha=1}^{N_p} S_\alpha = 1 \quad \text{(a saturation constraint)},\\
&\sum_{i=1}^{N_{cv}} c_{i\alpha} = 1 \quad (N_p \text{ phase concentration constraints}),\\
&c_i = \sum_{\alpha=1}^{N_p} S_\alpha c_{i\alpha} \quad (N_c \text{ component concentration constraints}),\\
&\hat{c}_j = \hat{c}_j(c_1, c_2, \ldots, c_{N_c}) \quad (N_{cv} \text{ adsorption constraints}),\\
&f_{i\alpha}(p_\alpha, T, c_{1\alpha}, \ldots, c_{N_c\alpha}) = f_{i\beta}(p_\beta, T, c_{1\beta}, \ldots, c_{N_c\beta})\\
&\quad (N_c(N_p - 1) \text{ phase equilibrium relations}),
\end{aligned} \tag{13}$$

where $f_{i\alpha}$ is the fugacity function of the ith component in the α phase.

For a general compositional flow, several EOSs (equations of state) can be used to define the fugacity functions $f_{i\alpha}$, such as the Redlich–Kwong, Redlich–Kwong–Soave, and Peng–Robinson EOSs. As an example, we describe the most used Peng–Robinson EOS.

Define, for $\alpha = 1, 2, \ldots, N_p$,

$$a_\alpha = \sum_{i=1}^{N_c}\sum_{j=1}^{N_c} x_{i\alpha} x_{j\alpha}(1 - \kappa_{ij})\sqrt{a_i a_j}, \quad b_\alpha = \sum_{i=1}^{N_c} x_{i\alpha} b_i,$$

where $x_{i\alpha}$ is the mole fraction of component i in phase α, κ_{ij} is a binary interaction coefficient between components i and j, and a_i and b_i are empirical factors for pure component i. The interaction coefficients account for molecular interactions between two unlike molecules. By definition, κ_{ij} is zero when i and j represent the same component, small when i and j represent components that do not differ much (e.g., when components i and j are both alkanes), and large when i and j represent components that are substantially different. Ideally, κ_{ij} depends on pressure and temperature and only on the identities of components i and j (Whitson 1982, Zudkevitch and Joffe 1970).

The factors a_i and b_i can be computed as follows:

$$a_i = \Omega_{ia}\alpha_i \frac{R^2 T_{ic}^2}{p_{ic}}, \quad b_i = \Omega_{ib}\frac{R\, T_{ic}}{p_{ic}},$$

where R is the universal gas constant ($R = 0.8205$), T is the temperature, T_{ic} and p_{ic} are the critical temperature and pressure, the EOS parameters Ω_{ia} and Ω_{ib} are given by

$$\begin{aligned}
&\Omega_{ia} = 0.45724, \quad \Omega_{ib} = 0.077796, \quad \alpha_i = \left(1 - \lambda_i\left[1 - \sqrt{T/T_{ic}}\right]\right)^2,\\
&\lambda_i = 0.37464 + 1.5423\omega_i - 0.26992\omega_i^2,
\end{aligned}$$

and ω_i is the acentric factor for components i. The acentric factors roughly express the deviation of the shape of a molecule from a sphere (Reid et al. 1977). We define

$$A_\alpha = \frac{a_\alpha p_\alpha}{R^2 T^2}, \quad B_\alpha = \frac{b_\alpha p_\alpha}{R\, T}, \qquad \alpha = 1, 2, \ldots, N_p, \tag{14}$$

where the pressure p_α is given by the Peng–Robinson two-parameter equation of state

$$p_\alpha = \frac{RT}{V_\alpha - b_\alpha} - \frac{a_\alpha(T)}{V_\alpha(V_\alpha + b_\alpha) + b_\alpha(V_\alpha - b_\alpha)}, \tag{15}$$

with V_α being the molar volume of phase α. Introducing the compressibility factor

$$Z_\alpha = \frac{p_\alpha V_\alpha}{R\,T}, \qquad \alpha = 1, 2, \ldots, N_p, \tag{16}$$

then equation (15) can be expressed as a cubic equation in Z_α:

$$Z_\alpha^3 - (1 - B_\alpha)Z_\alpha^2 + (A_\alpha - 2B_\alpha - 3B_\alpha^2)Z_\alpha - (A_\alpha B_\alpha - B_\alpha^2 - B_\alpha^3) = 0. \tag{17}$$

Now, for $i = 1, 2, \ldots, N_c$ and $\alpha = 1, 2, \ldots, N_p$, the fugacity coefficient $\varphi_{i\alpha}$ of component i in the mixture can be obtained from the equation

$$\ln \varphi_{i\alpha} = \frac{b_i}{b_\alpha}(Z_\alpha - 1) - \ln(Z_\alpha - B_\alpha) - \frac{A_\alpha}{2\sqrt{2}B_\alpha}\left(\frac{2}{a_\alpha}\sum_{j=1}^{N_c} x_{j\alpha}(1 - \kappa_{ij})\sqrt{a_i a_j} - \frac{b_i}{b_\alpha}\right)\ln\left(\frac{Z_\alpha + (1 + \sqrt{2})B_\alpha}{Z_\alpha - (1 - \sqrt{2})B_\alpha}\right). \tag{18}$$

Finally, the fugacity of component i is defined by

$$f_{i\alpha} = p_\alpha x_{i\alpha} \varphi_{i\alpha}, \quad i = 1, 2, \ldots, N_c,\ \alpha = 1, 2, \ldots, N_p. \tag{19}$$

3 Numerical methods

In our numerical method the temporal discretization is based on the backward Euler scheme, while the spatial discretization is based on the block-centered finite differences with the coefficients (e.g., the permeability $\mathbf{k}$) of differential equations harmonically averaged (equivalently, a mixed finite element method on rectangular parallelepipeds (Russell and Wheeler 1983). Our solution approach is evolved from the IMPEC that was used in (Delshad et al. 2000) for a compositional simulator of chemical flooding. The IMPEC solves for pressure implicitly and compositions explicitly. Due to the explicitness for the solution of the compositions, the size of time steps must be restricted to stabilize the overall procedure. In contrast, the approach employed here is a sequential approach that solves both the pressure and compositions implicitly. Hence this approach relaxes the time step restriction. The Newton–Raphson iterations for each of the pressure and composition equations are constrained by maximum changes in these variables over the iteration (Li et al. 2004), and an automatic time step size is determined by maximum changes over the time step (Chen et al. 2004, 2006). Upstream-weighted interblock flow (e.g., for mobilities) and injection/production terms are included. The linear system of algebraic equations is solved by the reduced band-width direct D4 method (Price and Coats 1974) or by the ORTHOMIN (orthogonal minimum residual, Vinsome 1976) or GMRES (generalized minimum residual (Saad and Schultz 1986) iterative method.

Both an implicit scheme in time for each of the pressure and composition equations and an implicit bottom-hole pressure treatment add stability and preserve user-specified rates and constraints. In fact, for the numerical tests carried out in the

next section, we have observed that the sequential approach is approximately twice faster than the IMPEC.

The sequential solution approach proceeds in the following order:

1. Solve the pressure equation implicitly.
2. Solve the transport system implicitly for the overall concentration of each component.
3. Use a chemical reaction equilibrium model to obtain the effective salinities.
4. Utilize a flash calculation to obtain the phase saturations and the concentrations of components in each phase.
5. Compute the interfacial tensions, trapping numbers, residual phase saturations, relative permeabilities, phase densities, viscosities, mobility reduction factors, etc.
6. Go back to step 1 to repeat this procedure until a final state is reached.

4 Numerical experiments

The chemical compositional model developed in the previous sections is applied to three experiments, a chemical flow without mass transfer between phases, a laboratory sandstone core, and an ASP+foam displacement problem with mass transfer. The purpose of the first experiment is to show that this chemical model is reliable and practical. Since there is no analytical solution available for the chemical compositional problem under consideration, the second experiment is utilized to compare numerical and laboratory results. The third experimental problem is more realistic than the first one, and is exploited to study oil recovery efficiency using different development methods, the oil displacement mechanisms, and the effects of different factors on ASP+foam flooding.

4.1 Example 1

This is a typical five-spot pattern problem with four injection wells and one production well; see Fig.1. The distance between the injection and production wells is 250 m. The number of horizontal grids is 9×9 with a spatial grid size of 44.19 m. The temporal step size is determined using an adaptive control strategy developed in Chen et al. (2004), and is of the order of several days, to ensure that the overall simulation procedure is stable. There are two layers in the vertical direction; the effective thickness of each layer is 3 m. The permeabilities in the first and second layers are 800 and 1,500 md, respectively, and the porosity is 0.26. The initial water saturation is 0.45, and

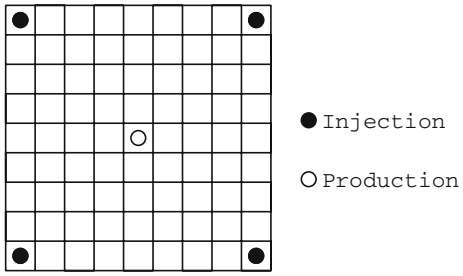

Fig. 1 A five-spot pattern

an injection rate of 0.19 PV/d is used. Water cut (WC) is defined as the ratio of water production to the sum of water and oil production.

The chemical simulator is applied to three types of injections: water, polymer, and ASP flooding. The injection modes are given below:

- Water flooding: Water is injected until WC= 98%.
- Polymer flooding: 0.05 PV water is injected, followed by polymer (1,000 ppm in solution) injection until the total injection reaches 0.38 PV, and then water is injected again until WC= 98%.
- ASP flooding: 0.05 PV water is injected, followed by ASP injection with 0.3% surfactant, polymer with 1,000 ppm in solution, and 2.0 wt % N_aOH until the total injection reaches 0.38 PV, and then water is injected again until WC= 98%.

The active function table of interfacial tension used in this simulation is given in Table 1. The recovery rates of the second (polymer flooding) and third (ASP flooding) types of injections are 23% and 32% OIP (oil in place), respectively. The WC curves for different injection methods are presented in Fig.2. Figures 3 and 4 display the residual oil saturation for the first layer using the polymer and ASP flooding, respectively, when WC equals 98%. Figure 2 shows that WC decreases to 79.85% and 66.56% from the highest value 92.34% for the second and third types, respectively, and that the third type reduces residual oil saturation much more dramatically than the second type does. These observations are in good agreement with physical intuition, and indicate that the chemical simulator is practical. While a quite coarse grid is utilized, an observation similar to that in Fig. 2 has been made for refined grids.

4.2 Example 2

To test the accuracy of our chemical compositional simulator, we now compare numerical results with laboratory results for a core flow experiment. It is a sandstone core, and it is inhomogeneous in the horizontal direction. The dimensions of

Table 1 The active function table of interfacial tension

\Surfactant Alkaline	0	0.001	0.002	0.003	0.004	0.005
0	20	0.9	0.2	0.12	0.07	0.04
0.5%	0.758	0.017	0.004	0.00019	0.00015	0.00010
1.0%	0.173	0.011	0.001	0.00009	0.00004	0.00003
1.5%	0.073	0.006	0.0007	0.00005	0.00003	0.00002
2.0%	0.03	0.002	0.0003	0.00002	0.00002	0.00001
3.0%	0.06	0.008	0.0007	0.00012	0.00010	0.00005

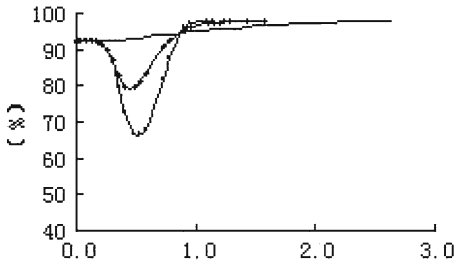

Fig. 2 Water cut vs. injected PV; water (top), polymer (middle), and ASP (bottom)

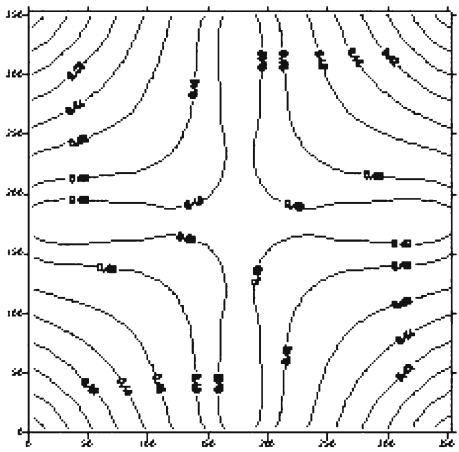

Fig. 3 Polymer flooding

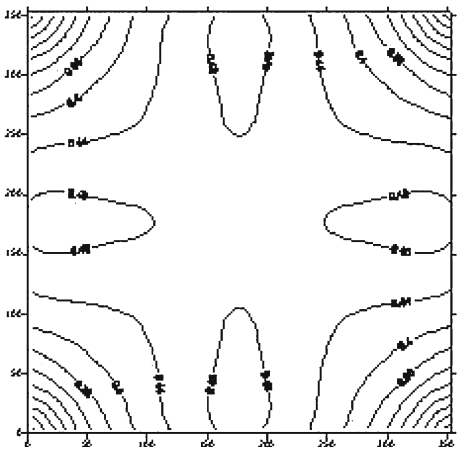

Fig. 4 ASP flooding

this core are $30 \times 4.5 \times 4.5$ cm^3; it has three layers, each having a thickness of 1.5 cm. The average permeability of each layer is 1,000 md, with a variation of 0.72. The porosity is 0.26, and water flooding has reached the stage of WC= 98%.

There are primary and secondary injections. In the primary injection, ASP consists of ORS41 with a concentration of 0.3%, 1.0 wt % N_aOH solution, and polymer 1275A with 2,000 ppm in solution; in the secondary injection, ASP is composed of ORS41 with a concentration of 0.05%, 1.0 wt % N_aOH solution, and polymer 1275A with 1,800 ppm in solution. These two injections are alternating equal-sized injections of (natural) gas and liquids, with 0.05 PV injected in each cycle. In the primary injection, the gas and liquids are injected 0.3 PV each; in the secondary, they are injected 0.1 PV each. After these two injections, there is a protection period. In this period, 0.05 PV polymer 1275A with 800 ppm in solution is first injected, then 0.15 PV polymer 1275A with 500 ppm in solution is injected, and water is finally injected. The oil recovery rates (relative to the current oil in place) obtained using the numerical simulation and laboratory experiment for this problem are shown in Fig. 5, and the corresponding WCs are presented in Fig. 6. These two figures show that the numerical and laboratory results match very well and the numerical simulation is accurate.

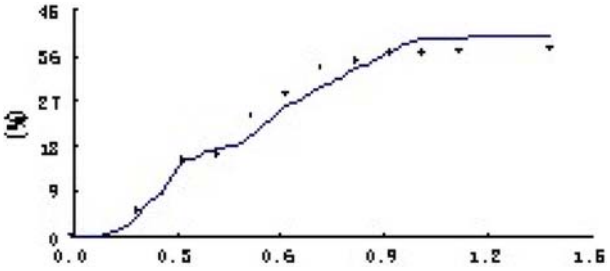

Fig. 5 Oil recovery vs. injected PV; numerical: – and laboratory · · ·

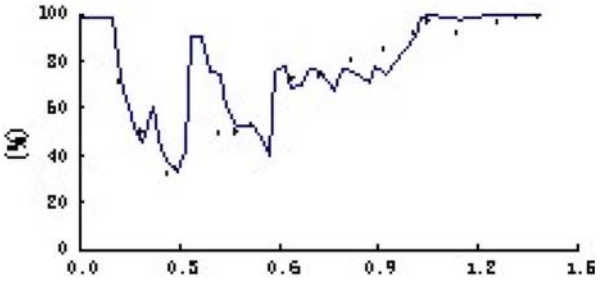

Fig. 6 Water cut vs. injected PV; numerical: – and laboratory · · ·

We remark that while the differential equations in the second section were derived for slightly compressible fluids, they do apply to the gas injection experiments in this article. The gas injection is studied in the context of ASP+foam flooding. In this type of flooding, on one hand, the polymer viscosity is quite large; on the other hand, due the presence of surfactants and foams, the emulsive phenomenon is significant. As a result, the viscosity of formed emulsions is substantially large and their mobility is really low. Therefore, in the entire ASP+foam flooding process, the oil reservoir considered is in a very high pressure. Under such a high pressure, most of gas flow in the form of foams, and their volume does not change much.

4.3 Example 3

This example is more realistic than the first example. We use the chemical compositional model to study oil recovery efficiency using different development methods, the oil displacement mechanisms, and the effects of different factors on ASP+foam flooding and to compare with UTCHEM.

4.3.1 The model

This is another five-spot pattern problem with one injection well and four production well, and the distance between the injection and production wells are 250 m (see Fig. 7). There are three vertical layers, each having a thickness of 2 m. The average permeability of the first, second, and third layers is 154, 560, and 2,421 md, respectively, with a variation of 0.72 on each layer. The porosity is 0.26, and the initial water saturation is 0.26. The number of grids used is $9 \times 9 \times 3$, and the horizontal grid size is 44.1942 m. The injection rate is 0.19 PV/d.

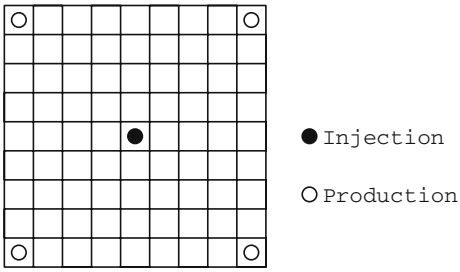

Fig. 7 Another five-spot pattern

4.3.2 Oil recovery study

The chemical compositional simulator is applied to four different injection methods: water, polymer, ASP, and ASP+foam flooding. These four injection procedures are described as follows:

- Water flooding: Water is injected until WC= 98%.
- Polymer flooding: Water is injected until $S_w = 0.915$, followed with polymer (1,000 ppm in solution) injection until the total injection reaches 0.57 PV, and then water is injected again until WC= 98%.
- ASP flooding: Water is injected until $S_w = 0.915$, followed with 0.015 PV polymer (1,000 ppm in solution) injection in a protection period, then ASP with 0.3% surfactant, 1.0 wt % NaOH, and polymer with 1,000 ppm in solution is injected until the total injection reaches 0.57 PV, and finally water is injected again until WC= 98%.
- ASP+foam flooding: Water is injected until $S_w = 0.915$, followed with 0.015 PV polymer (1,000 ppm in solution) injection in the protection period, then ASP+foam is injected with a simultaneous injection of gas and liquids, where the gas–liquid ratio is 1:1 and ASP+foam consists of 0.3% surfactant, 1.0 wt % NaOH, and polymer with 1,000 ppm in solution, until the total injection reaches 0.57 PV, and finally water is injected again until WC= 98%.

The oil recovery rates using these four injection methods are shown in Fig. 8. It follows from this figure that the ASP+foam flooding is the most efficient.

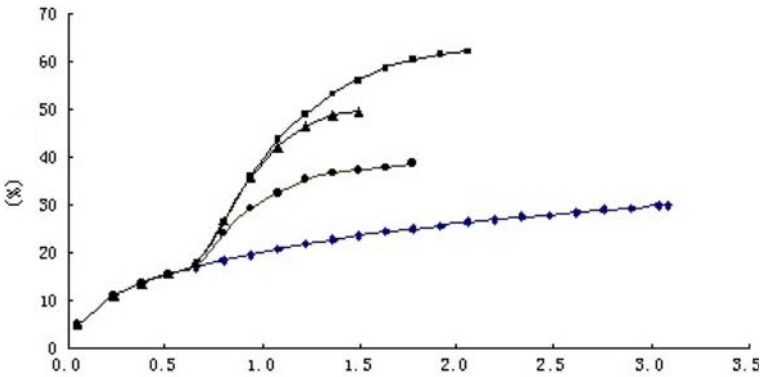

Fig. 8 Oil recovery vs. injected PV; water, polymer, ASP, and ASP+foam from bottom to top

4.3.3 Displacement mechanism study

As discussed in (Chen et al. 2006), in ASP+foam flooding for an initially oil-wet porous medium, because of a change of foam mobility resistance, ASP+foams enter the small pores that are not reached with water flooding and displace a large amount of residual oil there. Hence this type of flooding increases the efficiency of water flooding through larger volumetric sweep efficiency and a lower swept zone oil saturation.

Improving larger volumetric sweep efficiency is the ultimate goal of ASP+foam flooding in order to increase oil recovery of water, gas, or steam flooding in a petroleum reservoir. The improvement of this sweep efficiency heavily depends on the blocking capacity of foams in a porous medium. Numerical simulation is a useful approach in studying the mobility of ASP+foams in different permeability zones of the medium to determine the blocking role of foams.

In water flooding for a highly heterogeneous porous medium, most of the liquids are produced from high permeability zones, while a small amount of liquids are produced from low permeability zones. When foams are injected, they first enter the high permeability zones. As they are continually injected, they soon play a blocking role in these zones so that the mobility resistance there increases and then they gradually move to the low permeability zones. That is why a larger volume can be swept by this type of flooding.

We simulate water and ASP+foam flooding for the present problem. These two floodings and their injection slugs are given as follows:

- Water flooding: Water is injected until WC= 98%.
- ASP+foam flooding: Water is injected until $S_w = 0.915$, followed by 0.015 PV polymer (1,000 ppm in solution) injection in a protection period, then ASP+foam is injected with a simultaneous injection of gas and liquids, where the gas–liquid ratio is 1:1 and ASP+foam consists of 0.3% surfactant, 1.0 wt % N_aOH, and polymer with 1,000 ppm in solution, until the total injection reaches 0.57 PV, and finally water is injected again until WC= 98%.

The oil recovery rates of water and ASP+foam flooding are, respectively, 29.86% and 62.06% for the model problem considered. Obviously, the second flooding is far more efficient. Figures 9–11 give the liquid production in three different layers (high, intermediate, and low permeability layers) for these two floodings. It is clear from these figures that most of the liquids are produced from the high permeability layer, and less is produced from other two layers in water flooding. In ASP+foam flooding, foams can effectively block the high permeability layer so the liquid production decreases in this layer and increases in the intermediate and low permeability layers. In addition, the liquid production increases more in the intermediate permeability layer than in the low permeability. These observations agree with the displacement mechanism theory that a larger volume is swept by ASP+foam flooding.

4.3.4 Effects of different factors

Many factors affect oil recovery of ASP+foam flooding. Here we numerically study two of them: the gas–liquid ratio and different injection methods.

4.3.4.1. gas–liquid ratio effect. In ASP+foam flooding, the gas–liquid ratios are now set to be 1:1, 3:1, and 5:1. The oil recovery rates are given in Fig. 12 for these three cases.

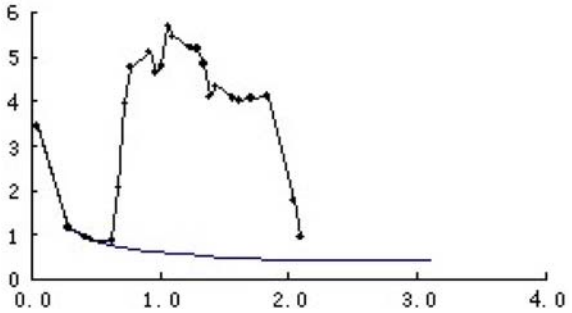

Fig. 9 Liquid production (m^3) vs. injected PV; water (bottom) and ASP+foam (top)

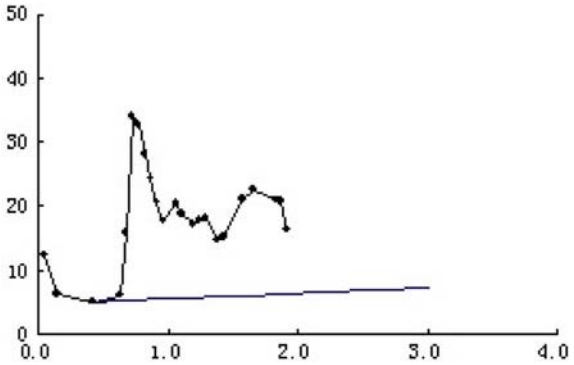

Fig. 10 Liquid production (m^3) vs. injected PV; water (bottom) and ASP+foam (top)

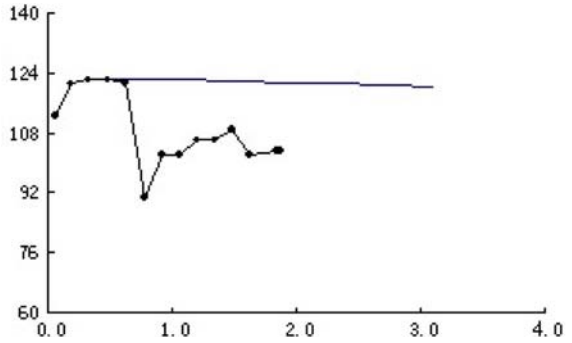

Fig. 11 Liquid production (m^3) vs. injected PV; water (top) and ASP+foam (bottom)

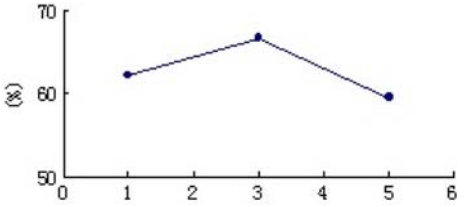

Fig. 12 Oil recovery vs. different gas–liquid ratios

It follows from this figure that the ratio 3:1 appears optimal. This ratio generates a good quality of foams, which can effectively enter and block the high permeability layer so that more displacing fluids can reach the intermediate and low permeability layers and thus larger volumetric sweep efficiency can be obtained.

4.3.4.2. Gas and liquid injection effect. The gas and liquid injections can be alternating or simultaneous. In addition, in the alternating injection, the injection frequency (or cycles) can be different. Different injection methods surely have different effects on oil recovery.

The gas–liquid ratio is fixed at 3:1. We study three injection methods: alternating injection with a low frequency, alternating injection with a high frequency, and simultaneous injection:

- Alternating with a low frequency: 0.095 PV ASP is injected, followed by 0.032 PV gas injection, then they are alternatingly injected until a cumulative ASP reaches 0.57 PV, and finally water is injected again until WC= 98%.
- Alternating with a high frequency: 0.0475 PV ASP is injected, followed by 0.0158 PV gas injection, then they are alternatingly injected until a cumulative ASP reaches 0.57 PV, and finally water is injected again until WC= 98%.
- Simultaneous injection: Gas and liquids are simultaneously injected until a cumulative ASP reaches 0.57 PV, and then water is injected again until WC= 98%.

The recovery rates for these three injection methods are displayed in Fig. 13. The numerical simulation shows that the simultaneous injection is more efficient than the alternating method. For the alternating method, the high frequency produces more than the low frequency does.

4.3.5 Comparison with UTCHEM

Finally, we use this example to compare our chemical compositional simulator with UTCHEM (Delshad et al., 2000). The ASP+foam flooding injection method in the oil recovery study (see Sect. 4.3.2) is used for the comparison, and the comparison results are displayed in Tables 2 and 3.

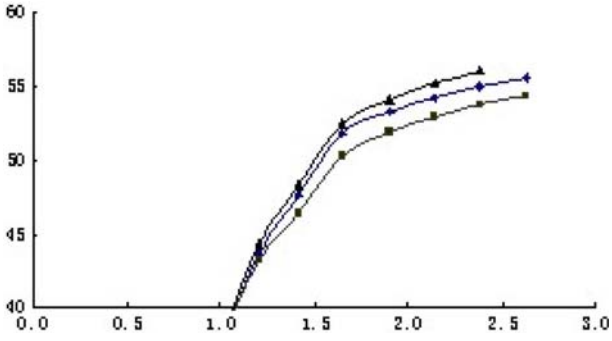

Fig. 13 Oil recovery vs. injected PV; alternating with low frequency (bottom), with high frequency (middle), and simultaneous (top)

Table 2 The sequential approach

Time (d)	Time step (d)	Courant number	Relative error of water conservation	Relative error of oil conservation
158.23	4.5231	0.5819	0.2516E−14	0.0
368.89	4.2427	0.4999	0.1309E−14	0.0
582.04	4.2803	0.4999	0.1909E−15	0.0
796.81	4.3092	0.4999	0.1592E−15	0.0
1,012.94	4.3349	0.4999	0.2729E−15	0.0
1,243.34	4.8795	0.5000	0.7106E−15	0.2244E−15
1,488.18	4.7864	0.5002	0.1713E−14	0.3315E−15
1,726.28	4.7537	0.5000	0.2827E−14	0.1336E−14
1,964.33	4.7700	0.5000	0.2763E−14	0.3724E−15
2,195.55	4.7823	0.5006	0.4592E−14	0.0
2,400.53	3.9473	0.5003	0.4337E−14	0.2940E−15
2,597.57	3.9749	0.4997	0.2530E−14	0.1470E−15
2,798.10	4.0313	0.4999	0.2126E−14	0.2352E−15

Table 3 The IMPEC approach

Time (d)	Time step (d)	Courant number	Relative error of water conservation	Relative error of oil conservation
50.19	0.7225	0.9987E−01	0.1492E−4	0.0
171.47	0.8352	0.9999E−01	0.2945E−5	0.0
297.62	0.8453	0.9999E−01	0.1946E−5	0.0
424.86	0.8509	0.1000	0.1599E−5	0.0
552.83	0.8552	0.1000	0.1244E−5	0.0
681.39	0.8588	0.1000	0.8808E−6	0.0
810.47	0.8622	0.1000	0.6652E−6	0.0
940.03	0.8653	0.1000	0.5305E−6	0.0
1,070.05	0.8682	0.1000	0.4391E−6	0.0
1,213.76	0.9777	0.1000	0.1703E−5	0.2460E−14
1,362.61	0.9892	0.1001	0.5009E−5	0.9660E−15
1,507.86	0.9596	0.1000	0.7801E−5	0.9379E−15
1,651.37	0.9549	0.1000	0.8495E−5	0.3478E−15
1,794.55	0.9547	0.1000	0.8380E−5	0.1659E−14
1,937.86	0.9561	0.1000	0.7962E−5	0.5047E−14
2,081.39	0.9577	0.1000	0.7407E−5	0.2156E−14
2,221.88	0.8596	0.1002	0.6831E−5	0.1705E−14
2,343.60	0.7966	0.1000	0.4803E−5	0.1235E−14
2,461.99	0.7854	0.1000	0.2005E−5	0.5292E−15
2,580.34	0.7943	0.9999E−01	0.4498E−6	0.7644E−15
2,700.20	0.8026	0.1000	0.1315E−6	0.5880E−15
2,780.61	0.8053	0.1000	0.8254E−7	0.2646E−15

Time steps in the simulations are controlled by the Courant number (see its definition in (Chen et al., 2006)). From Tables 2 and 3, we see that the Courant number is about 0.5 for the present sequential approach and it is about 0.1 for IMPEC. Accordingly, the time steps for the former are about 4–5 days, while they are less than 1 day for the latter. Also, the relative errors of water mass conservation are of order $\mathcal{O}(10^{-14})$ and $\mathcal{O}(10^{-5})$, respectively. On an SGI Origin 2000 computer, the total CPU times are, respectively, 130.1 and 207.6 s. Finally, the WCs obtained using both solution approaches are given in Fig. 14, and they match perfectly.

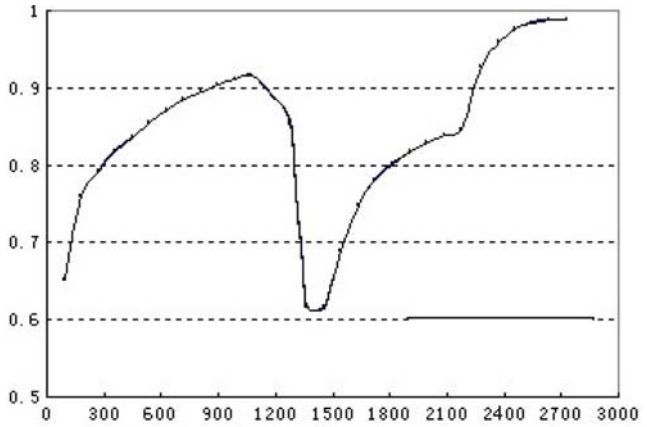

Fig. 14 Water cut vs. time (d); sequential: – and IMPEC: ···

5 Application to a Real Oilfield

In this section, the chemical compositional model is used to the numerical study and development prediction of a real oilfield. This oilfield is located in Asia, and has been operating since 1963.

5.1 Background

This oilfield is a large filed, but the area under study is 0.39 km^2, and the depth to its center is 935 m. Its porous volume is $64.05 \times 10^4, m^3$, and the initial OIP is 35.92×10^4 t. The initial pressure of the reservoir is 10.5 MPa. There are 16 wells; six are injection wells, and 10 are production wells. The average distance between the injection wells is 250 m, and the average distance between the injection and production wells is 176 m (Fig. 15). The central two production wells are the major producers, while other production wells are observatory. The control area, average effective thickness, porous volume, and initial OIP of the two major producers are 0.125 km^2, 6.8 m, 22.44×10^4 m^3, and 12.58×10^4 t, respectively. From March 1989 to September 1993, 36 periods of alternating water–gas injections were carried out. The cumulative gas injection is $4,938 \times 10^4$ m^3 (in standard conditions), equivalent to 0.24 PV; the cumulative water injection is 66.92×10^4 m^3, i.e., 0.48 PV.

5.2 The numerical model

To simulate this model problem, the injection and production wells are rearranged as in Fig. 15. A no-flow boundary condition is utilized. The reservoir has six layers, and the grid dimensions are $25 \times 17 \times 6$. The x_1- and x_2-spatial grid sizes are 31.304 and 30.829 m, respectively.

The effective thickness, permeability, porosity, and depth of the grid points where the wells are located are obtained from measurements and are given in Table 4. These data for other grid points are interpolated using the well grid points' data. The water saturation before ASP+foam flooding is not known. This saturation at well grid points can be measured using injection, liquid production, and WC data provided by

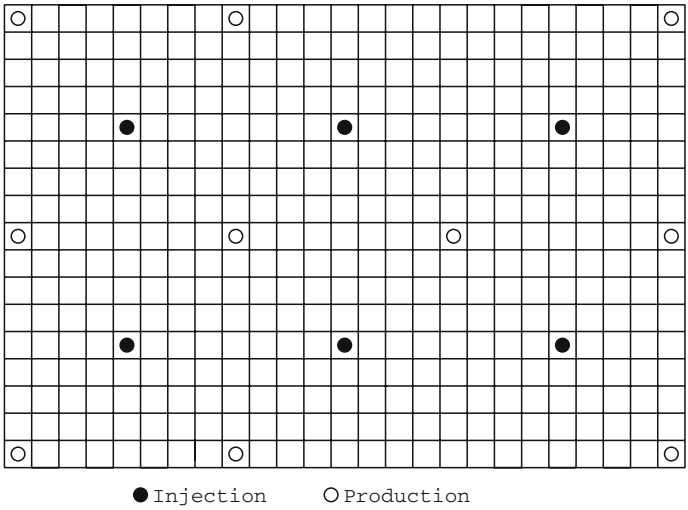

Fig. 15 The experimental area

Table 4 The reservoir data

	Effective thickness (m)	Permeability (μ^2m)	Porosity	Depth (m)
1st layer	0–2.8	0.04–0.378	0.235–0.257	912–950
2nd layer	0–1.4	0.039–0.417	0.235–0.257	914–952
3rd layer	0–2.8	0.04–0.596	0.235–0.257	920–953
4th layer	0.2–2.6	0.039–0.493	0.235–0.257	922–956
5th layer	0.5–2.2	0.039–0.543	0.235–0.257	924–958
6th layer	0–4.1	0.039–0.543	0.235–0.257	926–960

the wells. A WAG (water-alternating-gas) test was used to show that 13.88×10^4 m^3 of the injected gas is present in the reservoir before ASP+foam flooding. Since the gas injection region has a pore volume of 139.2×10^4 m^3, the ratio of these two numbers is 9.97%, which can be treated as a reference saturation of the remaining gas.

The physicochemical properties of chemical agents and foams used in this example are obtained from laboratory measurements combined with core flow experiments as in the second example of the previous section. The major properties of foams are: The critical water saturation equals 0.37, the critical concentration of surfactant is 0.0015, the critical oil saturation is 0.25, and the optimal gas–liquid ratio is 3:1. The active function of interfacial tension used is given in Table 1.

5.3 Numerical simulation-history matching

The numerical experiment involves the water flooding period of January 1–February 24, 1997, the pre-ASP flooding period of February 25–March 26, 1997, the major gas–liquid injection period of March 27, 1997–August 5, 1999, the secondary foam injection period of August 6, 1999–November 16, 2000, and the polymer (800 mg/l in solution) injection period of November 17, 2000–June 30, 2001. The gas and liquids are injected alternatingly. The injection modes are

- Pre-ASP flooding: 0.02 PV ASP is first injected, with 0.3% ORS41, 1.2 wt % N_aOH, and 15,000 (in thousand molecular weights) polymer with 1,200 mg/l in solution.
- Major ASP flooding: 0.55 PV ASP is injected, with 0.3% ORS41, 1.2 wt % N_aOH, and 15,000 (in thousand molecular weights) polymer with 1,200 mg/l in solution.
- Secondary ASP flooding: 0.3 PV ASP is injected, with 0.1% ORS41, 1.2 wt % N_aOH, and 15,000 (in thousand molecular weights) polymer and natural gas with 1,200 mg/l in polymer solution.
- Protection period: 0.1 PV polymer with 800 mg/l in solution is injected.

Polymer with 600 mg/l in solution has been injected in the current protection.

The central two production wells are the major producers so we will do a history matching only for these two producers. The history matching covers the period of January 1, 1997–June 30, 2001 from water flooding to the protection period of polymer injection. The matched variables include the daily oil and water production and WC. The history matching is performed through adjustment of relative permeabilities and other physical data. The matches between actual and numerical results for the matched variables are shown in Figs. 16–21 for the injected PV in the range 0–0.97 PV. The cumulative oil production for the period of January 1, 1997–June 30, 2001 is given in Table 5.

The relative error for WC match is 4.48%. From Figs. 16–21 and Table 5, other variables (daily oil and water productions, cumulative oil production, and recovery rate) also match very well.

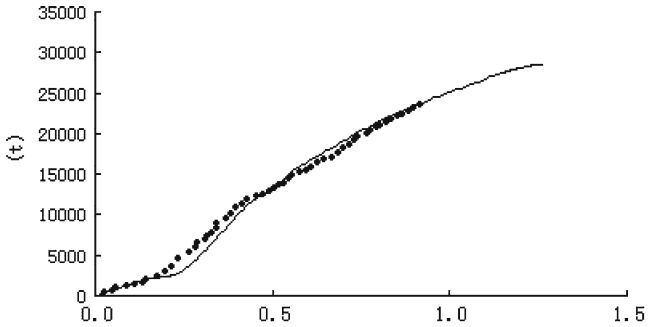

Fig. 16 Cumulative oil production vs. injected PV; numerical: – and actual · · ·

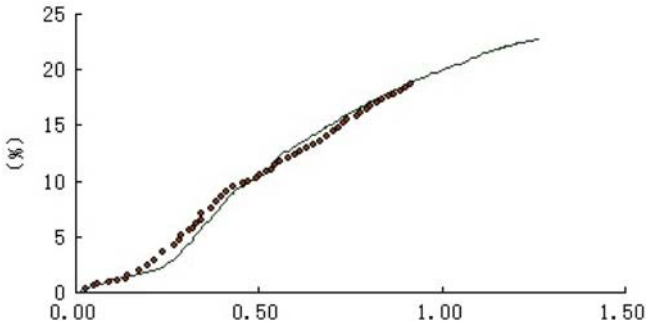

Fig. 17 Oil recovery vs. injected PV; numerical: – and actual · · ·

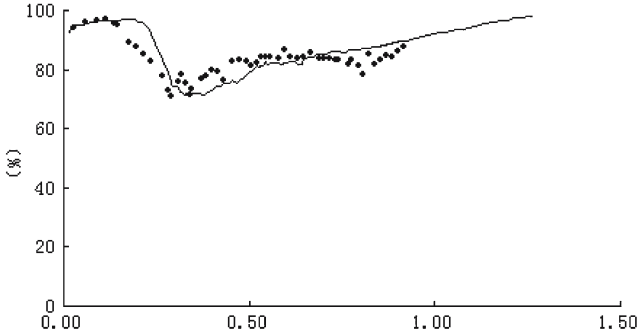

Fig. 18 Water cut vs. injected PV; numerical: – and actual · · ·

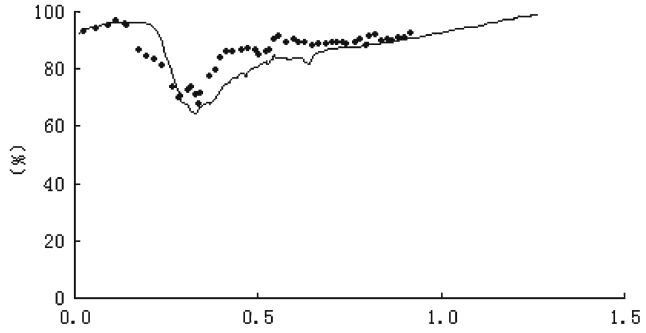

Fig. 19 Water cut vs. injected PV; numerical: – and actual · · ·

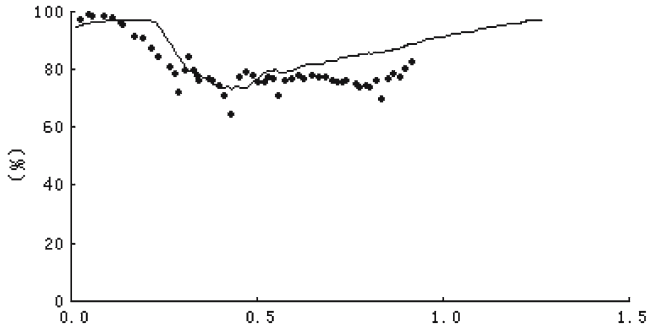

Fig. 20 Water cut vs. injected PV; numerical: – and actual · · ·

5.4 Predictions

We can employ the history matching-based adjusted model to predict the development and production of the present experimental region using ASP+foam flooding. The prediction is made until WC reaches 98%. The prediction for the central two producers is 28,603 t for the cumulative oil production, 22.74% for the recovery rate for the predicted time period, 67.36% for the recovery rate for the entire simulation time, and 1.27 PV for the injected PV (in the whole experimental oilfield). The predicted

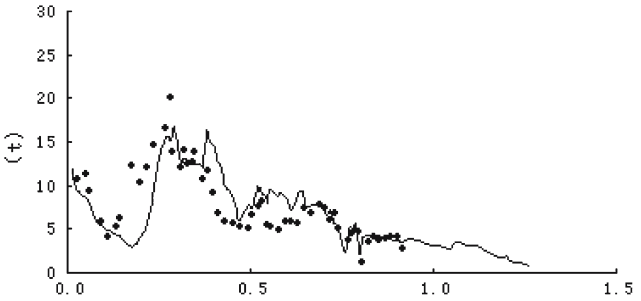

Fig. 21 Instantaneous oil production vs. injected PV; numerical: – and actual · · ·

Table 5 The history matching of cumulative oil production

	Cumulative production (t)	Recovery rates (%)
Actual	23,435	18.63
Numerical	23,647	18.80

results are displayed in Figs. 16–21, where the injected PV is in the range 0.97–1.27 PV.

5.5 Assessment of different development methods

One of the advantages of numerical reservoir simulation is its ability to assess different development methods for a petroleum reservoir in order to choose an optimal method, optimize oil and/or gas recovery, and achieve the most economic efficiency. For the present experiment, we compare three different development methods: water flooding, ASP+foam flooding with a protection period of polymer injection, and ASP+foam flooding without this protection period (i.e., water is further injected after the secondary ASP+foam flooding). The cumulative oil production and oil recovery rate for the predicted time period (January 1, 1997–June 30, 2001) are given in Table 6 for the two central producers. It follows from this comparison that it is very difficult to recover the remaining oil using water flooding alone. ASP+foam flooding recovers much more. Furthermore, the ASP+foam flooding with a protection period increases 1.26% in the recovery rate compared with one without the protection period. This implies that the second development project is the most efficient among the three projects.

Table 6 The assessment of different development methods.

	Cumulative production (t)	Recovery rates (%)
Water flooding	4,029	3.20
ASP+foam with protection	28,603	22.74
ASP+foam without protection	27,022	21.48

6 Concluding remarks

We have presented a three-dimensional model for multicomponent, multiphase chemical compositional flow in porous media. The model displays the main displacement mechanisms of chemical flooding such as interfacial tension lowering, capillary desaturation, chemical synergetic effects, and mobility control, involves dispersion, diffusion, adsorption, chemical reactions, and in situ generation of surfactant, and describes capillary trapping, cation exchange, and polymer and gel properties. A sequential numerical model evolved from an IMPEC numerical model developed by Delshad et al. Delshad et al. (2000) is described. For the numerical experiments in the previous section, we have observed that this sequential approach is about twice faster than the IMPEC. This simulation model can be used to design efficient development and production strategies in EOR and efficient remediation strategies in contaminant transport that account for realistic soil and fluid features. In this article, through its applications to three experiments and comparisons with laboratory results, this model has proven to be reliable, practical, and accurate. A real oilfield analysis has shown that it can accurately predict future oil production and recovery efficiency.

The comparisons between numerical and laboratory experiments and the applications to real oil fields performed in this article have indicated that (1) in practical applications, due to cost reasons, the concentration of surfactants used is below the critical micelle concentration (CMC). A new ASP+foam displacement mechanism for this type of system needs to be given through the synergetic effect of surfactant, alkaline, oil, and water (Chen et al., 2006). (2) From our experiments and measurements, the Langmuir-type isotherm is no longer valid, and the adsorbed surfactant concentration curve must be modified. (3) From our laboratory experiments, in the description of foam flooding the effect of relative permeabilities have been increased.

References

Bhuyan, D., Pope, G.A., Lake, L.W.: Mathematical modeling of high-pH chemical flooding. Proc. Soc. Pet. Eng. Int. Symp. on Oilfield chemistry, Anaheim, CA, Feb. 20–22, 1991.

Chen, Z., Huan, G., Li, B.: An improved IMPES method for two-phase flow in porous media. Transport Porous Media **54**, 361–376 (2004)

Chen, Z., Huan, G., Ma, Y.: Computational Methods for Multiphase Flows in Porous Media, Computational Science and Engineering Series, vol 2, SIAM, Philadephia, PA (2006)

Delshad, M., Pope, G.A., Sepehrnoori, K.: UTCHEM Version-9.0, Technical Documentation, Center for Petroleum and Geosystems Engineering. The University of Texas at Austin, Texas, July 2000.

Hirasaki, G.J.: Application of the theory of multicomponent, multiphase displacement to three-component, two-phase surfactant flooding. Soc. Pet. Eng. J. 191–204 (1981)

Hirasaki, G.J.: Interpretation of the change in optimal salinity with overall surfactant concentration. Soc. Pet. Eng. J. 971–982 (1982)

Lake, L.W.: Enhanced Oil Recovery. Prentice Hall, Englewood Cliffs, NJ (1989)

Li, B., Chen, Z., Huan, G.: Comparison of solution schemes for black oil reservoir simulations with unstructured grids. Comput. Meth. Appl. Mech. Eng. **193**, 319–355 (2004)

Meter, D.M., Bird, R.B.: Tube flow of non-Newtonian polymer solutions, Parts I and II-laminar flow and rheological models. AICHE J. 878–881, 1143–1150 (1964)

Morrow, N.R., Songkran, B.: In: Shah, D.O. (ed.) Surface phenomena in enhanced oil recovery. Plenum Press, New York City, pp. 387–411 (1982)

Pope, G.A., Nelson, R.C.: A chemical flooding compositional simulator. Soc. Pet. Eng. J. **18**, 339–354 (1978)

Price, H.S., Coats, K.H.: Direct methods in reservoir simulation. Soc. Pet. Eng. J. June, 295–308 (1974)

Reid, R.C., Prausnitz, J.M., Sherwood, T.K.: The Properties of Gases and Liquids, 3rd edn., McGraw-Hill, St. Louis (1977)
Russell, T.F., Wheeler, M.F.: In: Ewing, R.E. (ed.) Finite Element and Finite Difference Methods for Continuous Flows in Porous Media, the Mathematics of Reservoir Simulation. SIAM, Philadelphia, pp. 35–106 (1983)
Saad, Y., Schultz, M.H.: GMRES: a generalized minimal residual algorithm for solving nonsymmetric linear systems. SIAM J. Sci. Statist. Comput. **7**, 856–869 (1986)
Vinsome, P.K.W.: ORTHOMIN, an iterative method for solving sparse sets of simultaneous linear equations. In: Proc. Fourth Symposium on Reservoir simulations, Society of Petroleum Engineers of AIME, pp. 149–157 (1976)
Whitson, C.H.: Effect of physical properties estimation on equation-of-state predictions, paper SPE 11200, presented at the 57th Annual Fall Technical Conference and Exhibition of the Society of Petroleum Engineers of AIME, New Orleans, Louisiana (1982)
Zudkevitch, D., Joffe, J.: Correlation and prediction of vapor-liquid equilibria with the Redlich–Kwong equation of state. Am. Inst. Chem. Eng. J. **16**, 112–199 (1970)